Original article

MOLECULAR METABOLISM

Enhanced insulin sensitivity in skeletal muscle and liver by physiological overexpression of SIRT6*

Jason G. Anderson [1,7], Giorgio Ramadori [1,2,3,7], Rafael M. Ioris [2,3,7], Mirco Galiè [2], Eric D. Berglund [4,5], Katie C. Coate [5], Teppei Fujikawa [1], Stefania Pucciarelli [6], Benedetta Moreschini [6], Augusto Amici [6], Cristina Andreani [6], Roberto Coppari [1,2,3,*]

ABSTRACT

Objective: Available treatment for obesity and type 2 diabetes mellitus (T2DM) is suboptimal. Thus, identifying novel molecular target(s) exerting protective effects against these metabolic imbalances is of enormous medical significance. *Sirt6* loss- and gain-of-function studies have generated confounding data regarding the role of this sirtuin on energy and glucose homeostasis, leaving unclear whether activation or inhibition of SIRT6 may be beneficial for the treatment of obesity and/or T2DM.

Methods: To address these issues, we developed and studied a novel mouse model designed to produce eutopic and physiological overexpression of SIRT6 (Sirt6BAC mice). These mutants and their controls underwent several metabolic analyses. These include whole-blood reverse phase high-performance liquid chromatography assay, glucose and pyruvate tolerance tests, hyperinsulinemic-euglycemic clamp assays, and assessment of basal and insulin-induced level of phosphorylated AKT (p-AKT)/AKT in gastrocnemius muscle.

Results: Sirt6BAC mice physiologically overexpress functionally competent SIRT6 protein. While Sirt6BAC mice have normal body weight and adiposity, they are protected from developing high-caloric-diet (HCD)-induced hyperglycemia and glucose intolerance. Also, Sirt6BAC mice display increased circulating level of the polyamine spermidine. The ability of insulin to suppress endogenous glucose production was significantly enhanced in Sirt6BAC mice compared to wild-type controls. Insulin-stimulated glucose uptake was increased in Sirt6BAC mice in both gastrocnemius and soleus muscle, but not in brain, interscapular brown adipose, or epididymal adipose tissue. Insulin-induced p-AKT/AKT ratio was increased in gastrocnemius muscle of Sirt6BAC mice compared to wild-type controls.

Conclusions: Our data indicate that moderate, physiological overexpression of SIRT6 enhances insulin sensitivity in skeletal muscle and liver, engendering protective actions against diet-induced T2DM. Hence, the present study provides support for the anti-T2DM effect of SIRT6 and suggests SIRT6 as a putative molecular target for anti-T2DM treatment.

Keywords SIRT6 overexpression; Sirtuin; Insulin sensitivity; Glucose homeostasis; Diabetes

*Grants or fellowships supporting the writing of the paper: Coordenação de Aperfeiçoamento de Pessoal de Nível Superior (graduate student fellowship to R.M.I.), Juvenile Diabetes Research Foundation (Post-doctoral fellowship 3-2011-405 to T.F.), American Heart Association (Scientist Development Grant 14SDG17950008 to T.F.), European Commission (Marie Curie Career Integration Grant 320898 and ERC-Consolidator Grant 614847 to R.C.), and the Swiss National Science Foundation (310030_146533/1 to R.C.). This work has also received support from the Louis-Jeantet Foundation and the Fondation Pour Recherches Medicales of the University of Geneva (to R.C.).

[1]Department of Internal Medicine, Division of Hypothalamic Research, The University of Texas Southwestern Medical Center, Dallas, TX 75390, USA [2]Department of Cell Physiology and Metabolism, Faculty of Medicine, University of Geneva, 1211 Geneva, Switzerland [3]Diabetes Center of Faculty of Medicine, University of Geneva, 1211 Geneva, Switzerland [4]Advanced Imaging Research Center, The University of Texas Southwestern Medical Center, Dallas, TX 75390, USA [5]Department of Pharmacology, Howard Hughes Medical Institute, The University of Texas Southwestern Medical Center, Dallas, TX 75390, USA [6]School of Biosciences and Veterinary Medicine, University of Camerino, Via Gentile III da Varano, 62032 Camerino, Italy

[7] Co-first author.

*Corresponding author. Department of Cell Physiology and Metabolism, and Diabetes Center of the Faculty of Medicine, University of Geneva, 1211 Geneva, Switzerland. Tel.: +41 (0)22 3795539; fax: +41 (0)22 3795260. E-mail: roberto.coppari@unige.ch (R. Coppari).

Abbreviations: BAC, bacterial artificial chromosome; T2DM, type 2 diabetes mellitus; HCD, high-caloric diet; IPGTT, intraperitoneal glucose tolerance test; IPPTT, intraperitoneal pyruvate tolerance test; R_g, tissue-specific glucose uptake rate; GIR, glucose infusion rate; $EndoR_a$, endogenous glucose appearance rate; Rd, glucose disposal rate

Received June 7, 2014 • Revision received September 14, 2015 • Accepted September 15, 2015 • Available online 25 September 2015

http://dx.doi.org/10.1016/j.molmet.2015.09.003

1. INTRODUCTION

The prevalence of obesity and T2DM has risen significantly in the last decades. According to the World Health Organization T2DM and/or obesity are estimated to affect hundreds of millions worldwide (http://www.who.int/mediacentre/factsheets/fs311/en/ and http://www.who.int/mediacentre/factsheets/fs312/en/). Significant contributors to the rapid increase in the incidence of obesity and T2DM include recent lifestyle changes such as chronic consumption of hyper-caloric diets [1]. Unfortunately, current anti-obesity and -T2DM treatments are still suboptimal due to their side effects and the fact that long-lasting and debilitating morbidities (e.g.: heart disease, neuropathy, and hypertension) are still too often associated with these maladies [1–5]. Thus, development of more effective anti-obesity and -T2DM treatments is urgently needed. To these ends, the identification of novel molecular target(s) exerting protective effects against dietary obesity and/or T2DM is of paramount medical significance.

Recent genetic and pharmacological studies have identified sirtuins, which are nicotinamide adenine dinucleotide-dependent enzymes exerting post-translational modifications of their target proteins, as potential therapeutic targets for improving HCD-induced metabolic imbalances [6–15]. SIRT6, one of the seven mammalian sirtuins, is a lysine-deacetylase and mono-ADP-ribosyl-transferase with pleiotropic effects [16]. However, the role of SIRT6 in metabolism is controversial. For example, *Sirt6* knockout mice exhibit reduced adipose tissue mass and hypoglycemia [17]. SIRT6 deficiency also leads to attenuation of SIRT6-dependent transcriptional silencing resulting in increased expression of genes involved in glycolysis and glucose transport [18,19]. Of note, secretion of tumor necrosis factor-alpha (TNF-α), which is known to exert detrimental actions on energy homeostasis and insulin sensitivity [20], is diminished following knock-down of SIRT6 [21]. Therefore, according to these observations, systemic delivery of SIRT6 inhibitors should diminish adiposity, increase insulin sensitivity, glucose uptake and utilization, and consequently improve obesity and T2DM. However, in contrast to this notion, ubiquitous and supra-physiological overexpression of SIRT6 also leads to reduced adiposity and improved glucose metabolism in mice fed on a HCD [22]. Furthermore, adenoviral-mediated overexpression of SIRT6 in liver of diabetic mice suppresses hepatic glucose production and improves hyperglycemia [23]. Hence, these latter results suggest that systemic delivery of SIRT6 activators should bring about beneficial effects in the context of obesity and T2DM.

Based on the aforementioned data, it is unclear whether means to inhibit or enhance SIRT6 protein activity should be sought in order to treat obesity and/or T2DM. Also, the tissues underlying the effect of SIRT6 on whole-body glucose homeostasis are unknown. In order to address these issues, we developed and studied a novel mouse model designed to produce eutopic and physiological overexpression of SIRT6 (Sirt6BAC mice).

2. MATERIAL AND METHODS

2.1. Animals

Mice were housed with chow diet and water available *ad libitum* in light (12-hour light/12-hour dark cycles) and temperature (20–22 °C) controlled environments. Male mice were used for all experiments. Mice in HCD cohorts were fed a 58 kcal% fat w/sucrose diet (Open Source Diet Product #D12331 Research Diets Inc.) beginning at 8 weeks of age. Care of mice was within the Institutional Animal Care and Use Committee (IACUC) guidelines, and procedures were approved by the University of Texas Southwestern Medical Center IACUC and the ethical commission of the Canton of Geneva, Switzerland.

2.2. Generation of Sirt6BAC mice

A bacterial artificial chromosome (BAC) possessing 185.7 kb (70.7 kb upstream and 109.3 kb downstream) of unmodified mouse genomic DNA sequences flanking the *Sirt6* gene (BAC clone RP23-352G18, BACPAC RESOURCES, CHILDREN'S HOSPITAL Oakland, CA, USA) was purified as previously described [18] and used as template sequence for PCR reactions with the primer sets: 5′GACTGGGACCACACCAGAGT and 5′GTGAGAGCGGGAAGAGTACG; 5′AGGTGCCTGTGGACACTACC and 5′CAGGGGACACACTGGTTTCT; 5′CTGTCCACCTGTTGGAAGGT and 5′CTTCTGGGTCACCACAAGGT; 5′CATGAATGCTGTTTGGTTGG and 5′ATGCTGTAGGGTGGGAAGTG; 5′CCTTTGGAAAAGCAGTCAGC and 5′GAACTCCTGGCAAGTCGAAG; 5′CCACTGGGTCAGTCACACAC and 5′AGGACTCCACCTGGATTGTG. Upon observing the expected size of each amplicons, the purified BAC DNA was then electroporated into EL250 bacteria rendered electro-competent as previously described [24]. loxP sequences contained in the pBACe3.6 backbone of RP23-352G18 BAC DNA were replaced via homologous recombination [25] by an ampicillin resistance gene cassette generated via PCR amplification of a PGEM-T-Easy vector template with the primer sets: 5′GATAAACTACCGCATTAAAGCTTATCGATGATAAGCTGTCAAACATGAG-AATTGATCCGGATATATGAGTAAACTTGGTCTGAC and 5′GTTAACCGGGCTGCATCCGATGCAAGTGTGTCGCTGTCGACGGTGACC-CTATAGTCGAGGCGGTATTTTCTCCTTACGCATC. The modified RP23-352G18 BAC DNA was then purified and microinjected in its circular state into pronuclei of fertilized embryos of C57Bl/6J mice using standard methods [24]. By genotyping of tail biopsies using the following primer sets 5′TTGCTCTTGCGGGAAGCCCG and 5′GATACCGAGGGCGCCGTTCG (specific to the pBACe3.6 backbone sequence of RP23-352G18); 5′TTGCTGCATCAGGAGGGCGC and 5′TCCCACAATGCCCCGCTTCG (specific to the wild-type *Sirt6* allele) three mice were identified having germ-line incorporation of RP23-352G18 BAC DNA. These three Sirt6BAC mice were bred to wild-type C57Bl/6J mice establishing three distinct Sirt6BAC lines. Data shown here were obtained from the study of the line displaying two to four fold expression of SIRT6 compared to wild-type littermates.

2.3. Generation of Sirt6BAC; *Sirt6*$^{-/-}$ mice

Sirt6BAC mice were bred to mice heterozygous for the *Sirt6* null allele (*Sirt6*$^{+/-}$) [17]. F1 offspring were mated (*Sirt6*$^{+/-}$ × *Sirt6*$^{+/-}$; Sirt6BAC) to generate F2 breeder mice. From these F2 breeding pairs (*Sirt6*$^{+/-}$ × *Sirt6*$^{+/-}$; Sirt6BAC), F3 cohorts were obtained for experimental study including wild-types, mice harboring the Sirt6BAC (Sirt6BAC), or *Sirt6* knockout mice harboring Sirt6BAC (Sirt6BAC; *Sirt6*$^{-/-}$). To determine whether a mouse contained none, one, or two endogenous wild-type *Sirt6* sequences, we utilized a multiplex Taq-Man qPCR Copy Number genotyping analysis in which the commercially available Transferrin Receptor (*Tfrc*) (VIC dye-labeled probe) from Applied Biosystems (Foster City, CA, USA) was used as endogenous reference copy-number and the commercially available *Escherichia coli* β-galactosidase Mr00529369_cn (FAM dye-labeled probe) from Applied Biosystems (Foster City, CA, USA) was used to quantify the endogenous wild-type *Sirt6* allele copy number. Of note, the endogenous wild-type *Sirt6* sequences were swapped with the β-galactosidase sequences in *Sirt6*$^{+/-}$ mice [17]. Thus, mice bearing two of the endogenous wild-type *Sirt6* alleles were found to have zero copies of the β-galactosidase allele, whereas mice bearing one of the

endogenous wild-type *Sirt6* alleles were found to have one copy of the β-galactosidase allele, and mice lacking both of the endogenous wild-type *Sirt6* alleles were found to have two copies of the β-galactosidase allele.

2.4. Western blot

Tissues were lysed with RIPA buffer (R0278 Sigma Aldrich®) with 1:100 dilution of protease inhibitor cocktail (P8340 Sigma Aldrich®). Equal amounts of protein lysates (20 μg) were separated via SDS-PAGE and transferred to nitrocellulose membranes by electroblotting. Subsequently, the membranes were blocked using LI-COR® Odyssey® blocking buffer (927−40000) for 2 h at room temperature, then placed in primary antibody incubation (rabbit polyclonal anti-SIRT6 [Abcam® ab62739] 1:3000 dilution and mouse monoclonal anti-βActin [Sigma Aldrich® A5316] in LI-COR® Odyssey® blocking buffer w/0.1% Tween-20, overnight at 4 °C. After washing the membranes 3 × 10 min in PBS w/0.1% Tween-20, they were incubated at room temperature in darkness for 2 h with fluorescently conjugated secondary antibodies (goat anti-rabbit LI-COR® IRDye® 800CW [926−32211] 1:5,000 and goat anti-mouse LI-COR® IRDye® 680 [926−32220] 1:10,000) in Odyssey® blocking buffer w/0.1% Tween-20, 0.01%SDS. The membranes were imaged with a LI-COR® Odyssey® infrared imager. SIRT6 specific bands (~37kD) were quantified relative to housekeeping protein level using LI-COR® Odyssey® Image Studio software. p-AKT/AKT ratio was assessed as previously described [10].

2.5. Quantitative real-time PCR (qPCR)

Tissues were lysed in TRIzol® reagent in order to extract total RNA. cDNA was reverse transcribed from these purified RNA samples with Invitrogen SuperScript® III reverse transcriptase. Genes present on RP23-352G18 BAC were assayed via qPCR gene expression analysis to determine the levels of mRNA transcript expression. qPCR gene expression analysis was performed using inventoried TaqMan gene expression assays (Applied Biosystems®). These genes included: *AES* (Mm01148854_g1), *Ankrd24* (Mm01147213_m1), *BC025920* (Mm02763635_s1), *Gna11* (Mm01172792_m1), *Gna15* (Mm00494669_m1), *Tle2* (Mm00498094_m1), *Tle6* (Mm00475103_m1), and *Sirt6* (Mm01149042_m1). Expression levels were measured with an Applied Biosystems® 7900HT Sequence Detection System with SDS2.1 software. Baseline values of amplification plots were set automatically and threshold values were kept constant. The mRNA levels were expressed as arbitrary units and were obtained by dividing the averaged sample values (in triplicate) for each gene by that of the control housekeeper 18S rRNA (Mm03928990_g1).

2.6. Body weight and body composition

Mice were weighed every other week beginning at 8 weeks of age. Body composition was determined monthly beginning at 8 weeks of age using the EchoMRI-100™ quantitative nuclear magnetic resonance system providing precise measurements of whole body fat and lean mass.

2.7. Blood chemistry

Mice were singly housed in the morning (9am−12 pm) in cages with fresh bedding and access to water, but without food during this time period to ensure that the experimental measurements were not affected by postprandial effects. Fasting levels were gathered from blood samples obtained from mice fasted over-night. Glycemia measurements were taken from tail blood samples with OneTouch® Ultra® 2 glucometer with OneTouch® Ultra® Blue Test Strips. Immediately following, 50 μL of blood was collected in tubes at room temperature for five minutes before placing into ice. The blood samples were then centrifuged at 2,000 × g for 10 min at 4 °C. The blood serum supernatant was then pipetted into a new tube for storage at −80 °C. Blood chemistry was assessed as previously described [9,10,26].

2.8. Intraperitoneal glucose and pyruvate tolerance tests

Intraperitoneal glucose tolerance tests (IPGTT) and intraperitoneal pyruvate tolerance tests (IPPTT) were performed in male, age-matched mouse cohorts with similar body weights. Mice were singly housed and fasted overnight (6pm−10 am) in cages with fresh bedding and access to water, but without food during this time period to ensure that the experimental measurements were under fasting conditions. An hour before the *in vivo* experiment, mice were weighed to determine the dosage of glucose (1.5 g glucose per kg bodyweight) or pyruvate (2 g pyruvate per kg bodyweight) to be administered. Just prior to injecting the glucose (or pyruvate) bolus, fasting glycemia was measured from tail blood samples with an AlphaTRAK blood glucometer. The glucose (0.15 g glucose/mL 0.9% saline) or pyruvate (0.2 g sodium pyruvate/mL 0.9% saline) solution was then injected into the intraperitoneal cavity of each mouse. Blood glucose measurements were taken from tail blood samples at times indicated in the figures.

2.9. Hyperinsulinemic-euglycemic clamp

Clamp was performed in male, standard chow-fed, age-matched mice with similar body weights. 5 days prior to the experiment, mice were anesthetized using isoflurane and a catheter was surgically implanted in the right jugular vein and exteriorized above the neck as previously described [27]. Hyperinsulinemic-euglycemic clamps were then performed in these 14−16 week old, conscious, unrestrained catheterized mice. Mice were fasted 5 h prior to the start of the experiment (t = 0 min). At t = −120 min, an infusion of [3-^{3}H]glucose (0.05 μCi/min) was initiated. At t = −15 and −5 min, blood samples were collected from the tail vein to measure basal blood glucose and plasma insulin as well as to calculate the rate of endogenous glucose appearance (EndoR_a) and glucose disposal (R_d). At t = 0 min, a continuous insulin infusion (4 mU/kg bodyweight/min.) was used to induce hyperinsulinemia and the infusion of [3-^{3}H]glucose was increased to 0.1 μCi/min. Blood samples were then taken every 10 min to measure blood glucose, and 50% dextrose was infused as needed to maintain target euglycemia (120 mg/dL). This target was chosen because it was the average basal glycemia of the two groups. Additional blood samples were taken every 10 min from t = 100−120 min (steady state clamp) to determine plasma insulin and calculate glucose turnover. After the blood sample was taken at t = 120 min, a 13 μCi bolus of 2[^{14}C]deoxyglucose tracer was administered for the measurement of tissue-specific glucose uptake (R_g). Blood samples were obtained at t = 122, 130, 137, 145 min to assess blood glucose and 2[^{14}C]deoxyglucose specific activity. Mice were then anesthetized using chloral hydrate. Brain, interscapular brown adipose tissue, liver, epididymal white adipose tissue, gastrocnemius, and soleus muscle were flash-frozen in liquid nitrogen for storage at −80 °C for further analysis. Plasma concentrations of [3-^{3}H]glucose were determined following deproteinization of plasma samples with zinc sulfate and barium hydroxide. Basal glucose turnover and insulin-stimulated R_d was determined as the ratio of the [3-^{3}H]glucose infusion rate to the specific activity of plasma [3-^{3}H]glucose at the end of basal period and during clamp steady state, respectively. EndoR_a during the clamp was determined by subtracting steady state GIR from R_d. R_g was determined by measuring the accumulation of phosphorylated 2[^{14}C]

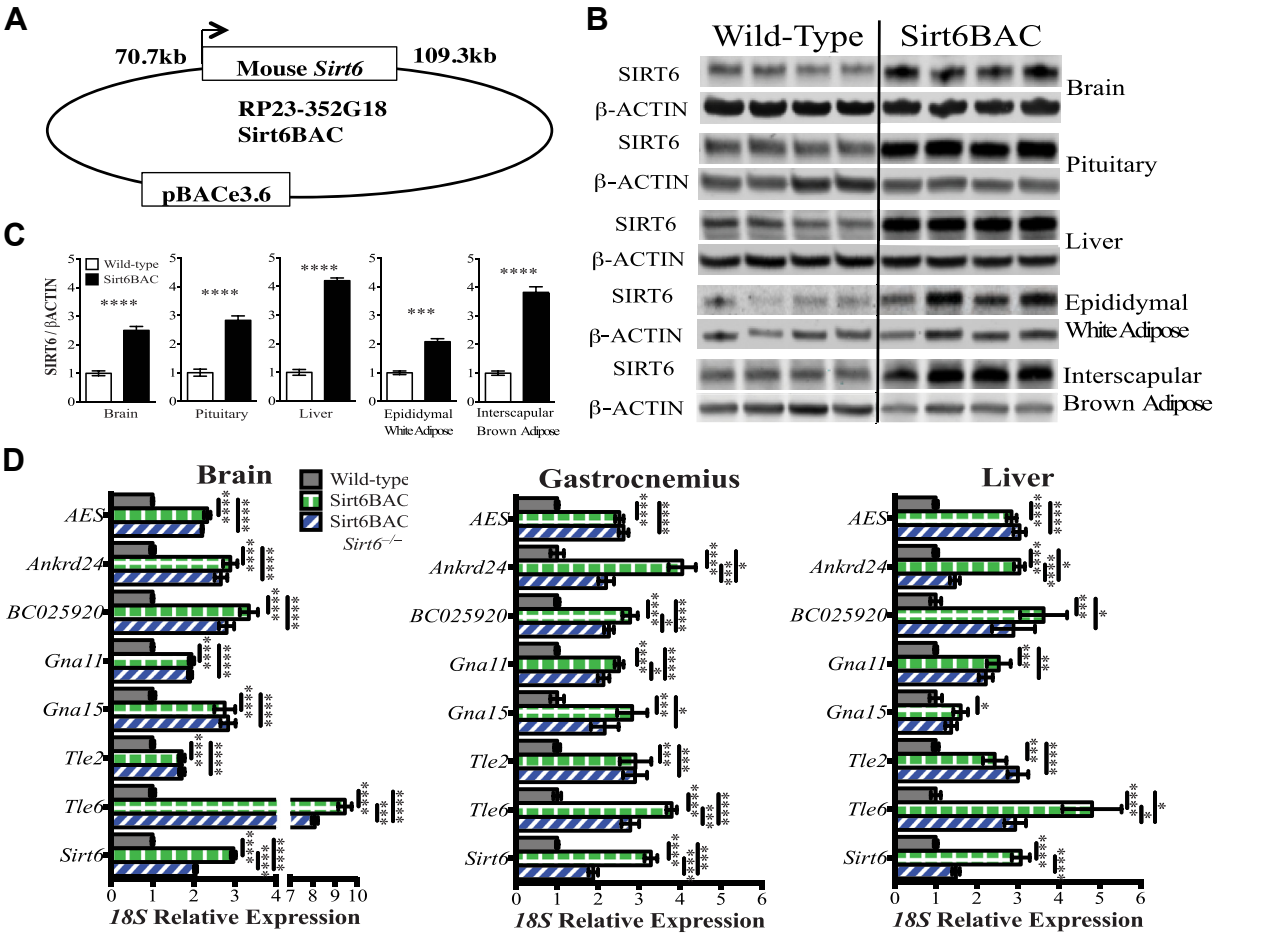

Figure 1: Sirt6BAC mice eutopically overexpress mouse SIRT6. **(A)** Schematic representation of the RP23-352G18 (BACPAC Resources, Children's Hospital Oakland Research Institute) BAC DNA construct containing the mouse *Sirt6* gene used to generate Sirt6BAC mice. **(B)** Anti-SIRT6 Western blots of tissues from Sirt6BAC and wild-type standard-diet-fed mice on a pure C57Bl/6 genetic background. (Each lane represents tissue from a single mouse). For each tissue, data were gathered from the same membrane. The same membrane was digitally separated to improve clarity. **(C)** Quantification of the relative SIRT6/βACTIN expression shown in panel B (n = 4 per group). **(D)** qPCR measurements of brain, gastrocnemius and liver gene transcripts present in wild-type, Sirt6BAC, and Sirt6BAC; *Sirt6*$^{-/-}$ standard-diet-fed mice on a C57Bl/6; 129SvJ mixed genetic background (n = 6–8 per group). Values are mean ± S.E.M. Statistics were analyzed using unpaired two-tailed t-test when 2 groups were compared and one-way ANOVA with Tukey correction for multiple comparisons when 3 or more groups were compared (*p < 0.05, **p < 0.01, ***p < 0.001, ****p < 0.0001).

deoxyglucose in dissected tissues and the disappearance of 2[^{14}C] deoxyglucose from blood.

2.10. Reverse phase high-performance liquid chromatography (RP-HPLC)

Blood was collected from 2-month-old male standard-diet-fed mice and then treated with 10 μL of 1% EDTA. In order to detect polyamines through RP-HPLC, blood samples underwent a dansylation procedure. 100 μl of blood (previously treated with 5% TCA to allow protein precipitation) and 1 ml of standard polyamines stock solutions (1 mg/ml) were subjected to a derivatization process with dansyl chloride according to Seiler [28]. After incubation at 40 °C for 45 min with dansyl chloride, mixtures were filtered through a 0.45 μm RC-membrane (ALBET-LabScience, Dassel/Relliehausen, Germany) and injected into a HPLC apparatus (Agilent 1100) for analysis. The separation was executed on a Supelcosil LC 18 RP column (5 μm; 4,6 × 250 mm) maintained at 35 °C. The mobile phase was composed of water and methanol with the gradient elution system at a flow rate of 1.0 ml/min. The initial mobile phase contained 70% methanol for 7 min. The gradient volume of methanol was 70–75% at 7–10 min, 75–90% at 10–20 min and 90–100% at 20–25 min. The signal detection was through a Diode Array Detector (DAD) and the chromatograms were recorded at a wavelength of 253 nm. Polyamines calibration curves were obtained using dansylated polyamine standard solutions (concentrations ranging between 0.001 mg/ml and 0.1 mg/ml). Polyamines concentration was normalized to total protein concentration obtained with Bradford assay and expressed as nmol/mg.

2.11. Statistical analyses

Data are reported as mean ± SEM. All statistical analyses were performed using Graphpad Prism® 6.0c software. Unpaired two-tailed t-tests were employed when 2 groups were compared, and one-way ANOVA with Tukey correction for multiple comparisons were employed when 3 or more groups were compared, and repeated measures two-way ANOVA with Tukey correction for multiple comparisons were used when 3 or more groups were compared over a time-course.

3. RESULTS

3.1. Generation and validation of Sirt6BAC mice

To determine the role of SIRT6 on energy and glucose homeostasis, we generated genetically-engineered mice harboring bacterial artificial chromosome (BAC) DNA containing 70.7 kb upstream and 109.3 kb downstream sequences flanking the mouse *Sirt6* gene (Sirt6BAC mice) (Figure 1A). In several tissues of Sirt6BAC mice, SIRT6 protein level was found to be two to four times greater than wild-type controls (Figures 1B,C and S1), suggesting that DNA sequences contained in the BAC include the crucial transcriptional regulatory elements of the endogenous *Sirt6* gene. Of note, this magnitude of SIRT6 overexpression found in Sirt6BAC mice is physiological as it approximates that which is observed in calorically restricted rodents [29].

Virtually all BAC-based transgenic approaches suffer from two major confounders that may alter gene expression and hence cause phenotypes: 1) the presence of additional coding and/or non-coding sequences contained in the large BAC DNA sequences and 2) DNA construct insertion site into the genome. As the genomic fragment used to generate Sirt6BAC mice bears additional known mouse genes (i.e.: *AES, Ankrd24, BC025920, Gna11, Gna15, Tle2,* and *Tle6*), we assessed their mRNA contents and found them to be increased in Sirt6BAC mice compared to wild-types (Figure 1D). Hence, to disassociate the effect of SIRT6 overexpression from the potential effect of non-SIRT6 BAC-born products and/or BAC insertion site(s) on a given phenotype, we generated an additional control genotype. This was accomplished by breeding the Sirt6BAC allele to the *Sirt6* null (*Sirt6*$^{-}$) allele [17]. This breeding scheme produced three experimental genotypes that were used in this study: 1) wild-type, 2) Sirt6BAC, and 3) Sirt6BAC; *Sirt6*$^{-/-}$ mice. Of note, quantitative PCR profiling of brain, gastrocnemius and liver indicated that while *AES, Ankrd24, BC025920, Gna11, Gna15, Tle2,* and *Tle6* mRNA levels are similarly increased in Sirt6BAC and Sirt6BAC; *Sirt6*$^{-/-}$ mice the latter showed reduced *Sirt6* mRNA level compared to the former genotype (Figure 1D). Also, while SIRT6 protein level is significantly increased in several tissues of Sirt6BAC mice compared to wild-type controls (Figures 1B,C and S1), it is similar between gastrocnemius of Sirt6BAC; *Sirt6*$^{-/-}$ mice and wild-type controls (Figure S1).

To validate the functional competence of BAC-DNA-derived SIRT6 protein, the ability of Sirt6BAC allele to rescue the phenotypes displayed by *Sirt6*$^{-/-}$ mice was assessed. Among other defects, *Sirt6*$^{-/-}$ mice have increased early-postnatal mortality and reduced body length and weigh compared to wild-type mice [17]. These aberrancies were all rescued by introduction of Sirt6BAC allele in the *Sirt6* null background. Indeed, while viability, body length and weight were all reduced in *Sirt6*$^{-/-}$ mice (as predicted) all these parameters were found to be normal in Sirt6BAC; *Sirt6*$^{-/-}$ mice (Figure 2A–C). Collectively, these data demonstrate that Sirt6BAC mice physiologically overexpress functionally competent SIRT6 protein.

3.2. Normal energy balance in Sirt6BAC mice

To determine the effect of physiological overexpression of SIRT6 on energy homeostasis, we measured body weight and composition of Sirt6BAC mice, and Sirt6BAC; *Sirt6*$^{-/-}$ and wild-type controls either fed on a standard chow or on a HCD. In both feeding contexts, body weight, fat and lean mass were all similar between Sirt6BAC, Sirt6-BAC; *Sirt6*$^{-/-}$, and wild-type mice (Figure 3A–F). Together, these data demonstrate that physiological overexpression of SIRT6 neither affects energy homeostasis nor protects from, or predisposes to, developing diet-induced obesity.

3.3. Improved glucose homeostasis in Sirt6BAC mice

To determine the impact of physiological overexpression of SIRT6 on glucose homeostasis, we measured several parameters of glucose metabolism in Sirt6BAC mice and controls. Data shown in Figure 4A indicate that in standard chow and HCD feeding conditions, 16-week-old Sirt6BAC mice have reduced circulating glucose levels compared to controls indicating that these mice are protected from developing diet-induced T2DM. Of note, circulating glucose levels were not different between Sirt6BAC; *Sirt6*$^{-/-}$ and wild-type HCD-fed mice (Figure 4A) hence suggesting that the glycemia phenotype shown by Sirt6BAC mice is very likely the result of SIRT6 overexpression. The improved hyperglycemia concomitant with unchanged circulating fed (Figure 4B) and fasting (ng/mL; mean $\pm$ SEM: wild-types $=$ 0.53 $\pm$ 0.058; Sirt6BAC mice $=$ 0.51 $\pm$ 0.02; Sirt6BAC; *Sirt6*$^{-/-}$ mice $=$ 0.53 $\pm$ 0.060; n $=$ 9–15 per group, $p > 0.05$) insulin level hinted that Sirt6BAC mice may exhibit enhanced insulin sensitivity.

To further investigate the effects of SIRT6 overexpression on glucose metabolism, Sirt6BAC mice and controls were assessed for pyruvate and glucose tolerance. In both feeding conditions, Sirt6BAC mice exhibited reduced glycemic excursions during these tests (Figure 4C–F). Of note, the improved pyruvate and glucose handling were more pronounced in the HCD feeding context. These phenotypes of Sirt6BAC mice are very likely the result of SIRT6 overexpression because Sirt6BAC; *Sirt6*$^{-/-}$ mice displayed intermediate degrees of glycemic excursions during these tests (Figure 4C–F). Collectively, our data indicate that physiological overexpression of SIRT6 reduces glycemia and improves the glucose imbalance brought on HCD feeding.

A

Genotype	n	Mendelian Ratio Observed	Mendelian Ratio Expected	Observed / Expected
Wild-type	36	0.138	0.125	110.8%
Sirt6BAC	35	0.135	0.125	107.7%
Sirt6BAC; *Sirt6*$^{-/-}$	37	0.142	0.125	113.8%
Sirt6$^{-/-}$	9	0.035	0.125	27.7%

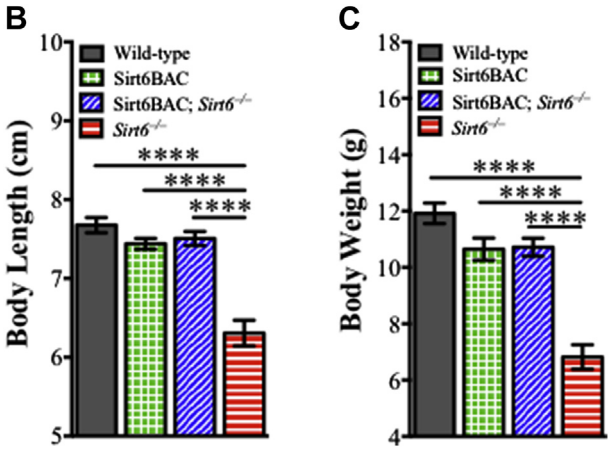

Figure 2: SIRT6 generated from Sirt6BAC is functionally competent. (A) Frequency of viable mice per genotype observed at 4-week of age, shown as a percentage of the expected Mendelian ratio. Mice were fed on a standard diet. **(B)** Body length (n $=$ 9–13 per group) and **(C)** body weight (n $=$ 9–13 per group) of 3-week-old mice fed on a standard diet. Values are mean $\pm$ S.E.M. Statistics were analyzed using one-way ANOVA with Tukey correction for multiple comparisons (****$p < 0.0001$).

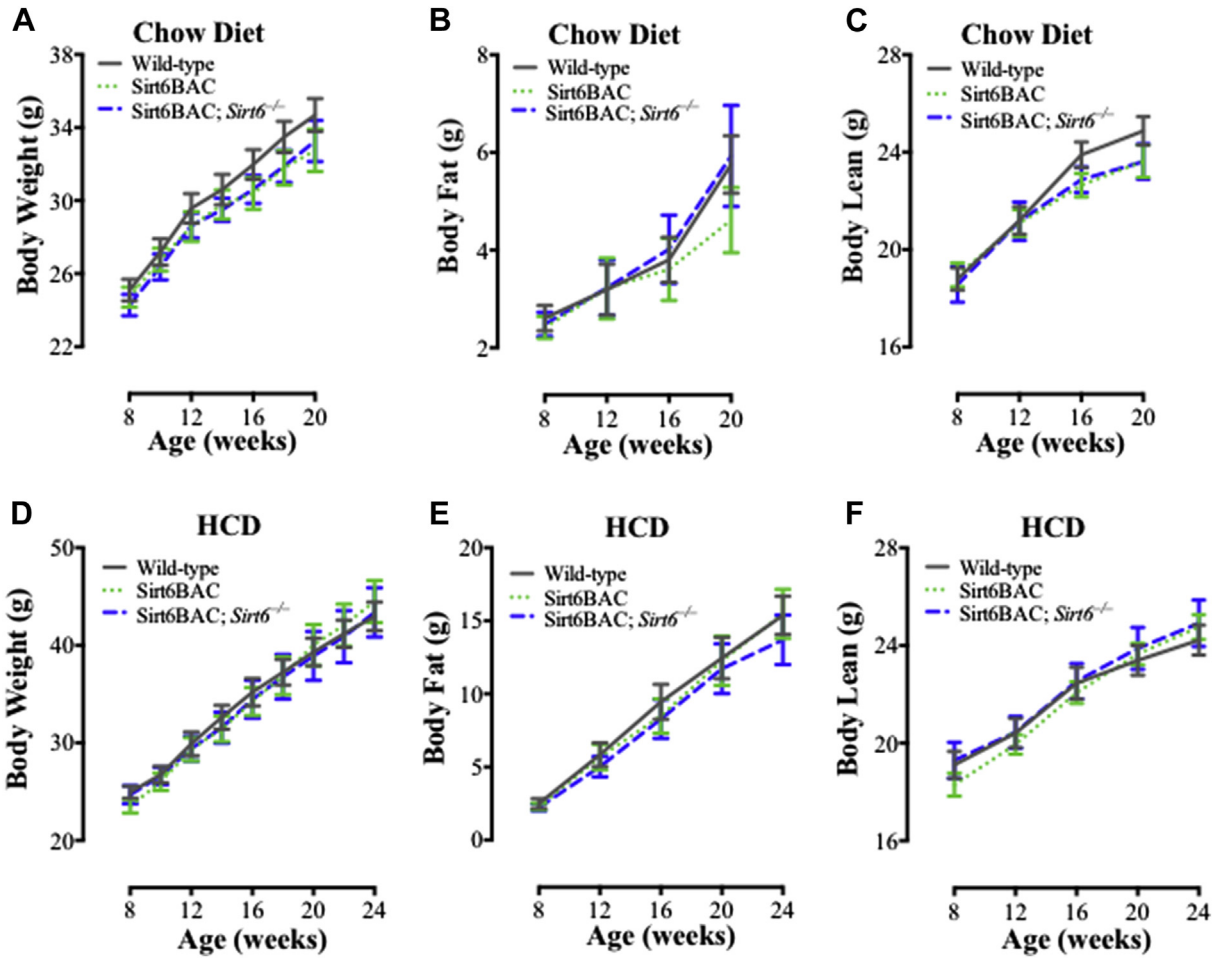

Figure 3: Sirt6BAC mice display normal body weight, fat mass and lean mass. **(A)** Body weight, **(B)** body fat weight, and **(C)** body lean weight of mice in chow diet context (n = 14–21 per group). **(D)** Body weight, **(E)** body fat weight, and **(F)** body lean weight of mice in HCD context (n = 10–14 per group). Values are mean ± S.E.M. Statistics were analyzed using a repeated measures two-way ANOVA with Tukey correction for multiple comparisons.

3.4. Enhanced insulin sensitivity in liver and skeletal muscle of Sirt6BAC mice

One possible explanation for the improved glucose homeostasis displayed by Sirt6BAC mice is enhanced insulin sensitivity. To directly test this hypothesis, hyperinsulinemic-euglycemic clamp assays were performed. During the clamp, insulin was infused to achieve hyperinsulinemia while D-glucose was infused through the same intravenous line at modulated rates to maintain euglycemia. In agreement with the aforementioned data suggestive of increased insulin sensitivity of Sirt6BAC mice, the glucose infusion rate (GIR) (Figure 5A) needed to clamp euglycemia (Figure 5B) was greatly increased in chow-fed Sirt6BAC mice compared to wild-type littermates. Basal endogenous glucose appearance rate (EndoR_a) (Figure 5C) and basal glucose disposal rate (R_d) (Figure 5D) were not significantly different between Sirt6BAC mice and wild-type controls. During the clamp however, the ability of insulin to suppress endogenous glucose production was significantly enhanced in Sirt6BAC mice compared to wild-type controls (Figure 5C). Insulin-stimulated glucose disposal was also increased in Sirt6BAC mice compared to wild-type controls (Figure 5D).

To determine the relative contributions of certain tissues to glucose disposal, the amounts of exogenously administered radiolabeled glucose analog 2[^{14}C]deoxyglucose were measured in several tissues. As shown in Figure 5E, insulin-stimulated glucose uptake was enhanced in Sirt6BAC mice in both gastrocnemius and soleus muscle, but not in brain, interscapular brown adipose, or epididymal adipose tissue. The whole-body glycolytic rate as percent of glucose disposal (Figure 5F) was not found to be significantly different between genotypes. Overall, these data demonstrate that insulin sensitivity is selectively augmented in liver and skeletal muscle of Sirt6BAC mice.

To independently assess *in vivo* insulin sensitivity, we used a well-established biochemical approach. The level of phosphorylated AKT (p-AKT) following a bolus of insulin has been used as measure of the ability of the hormone to activate its receptor [10]. Intraperitoneal insulin administration enhanced p-AKT/AKT ratio in gastrocnemius of Sirt6BAC, Sirt6BAC; *Sirt6*$^{-/-}$, and wild-type mice (Figure 6A,B). Of note, while the ability of insulin to induce phosphorylation of AKT was significantly increased in gastrocnemius of Sirt6BAC compared to wild-type mice (Figure 6A), it was not different between Sirt6BAC; *Sirt6*$^{-/-}$ and wild-type controls (Figure 6B). These results are in keeping with data shown in Figure 5E and further support the idea that SIRT6 overexpression drives enhanced insulin sensitivity in Sirt6BAC mice.

3.5. Increased spermidine content in blood of Sirt6BAC mice

To gather insights on potential mechanisms by which SIRT6 overexpression boosts insulin sensitivity we surveyed hepatic gene

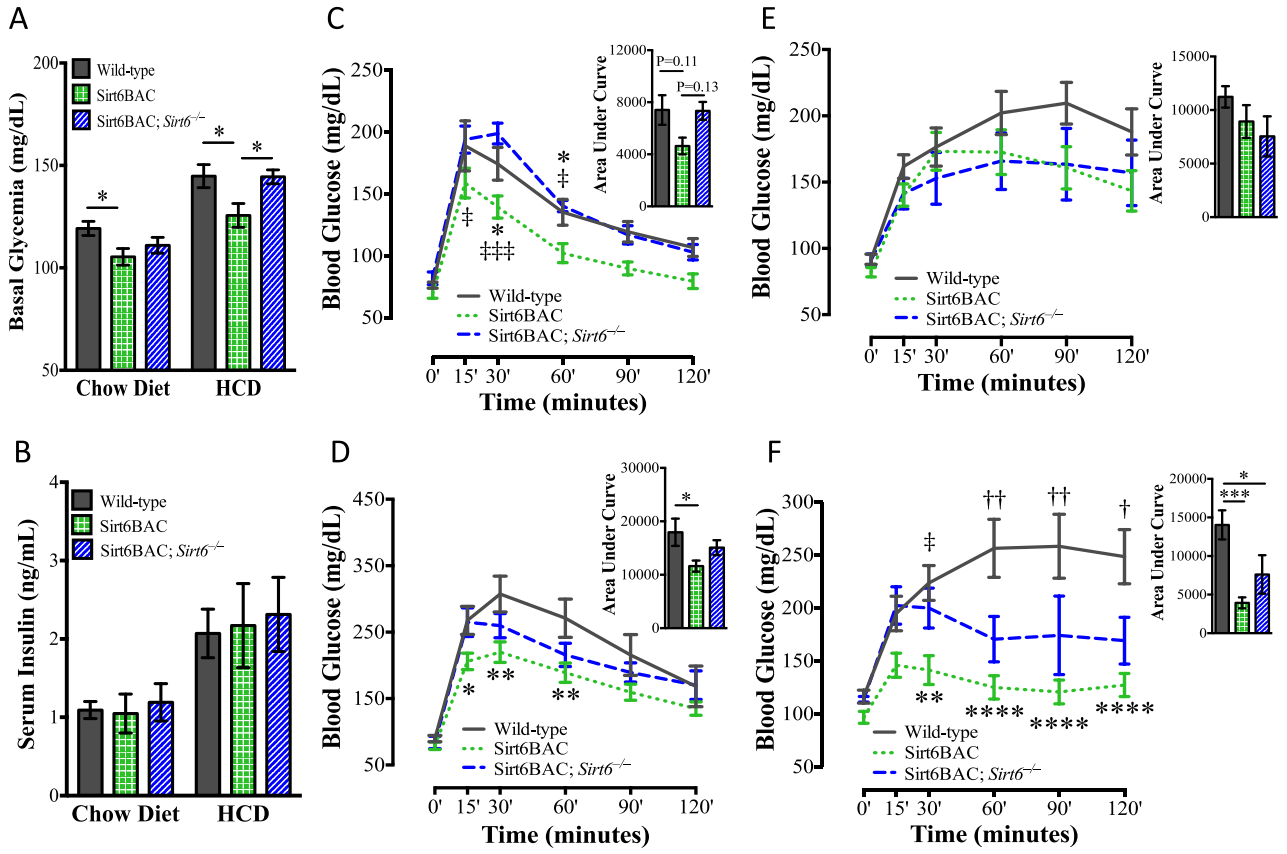

Figure 4: Sirt6BAC mice exhibit improved glucose homeostasis. **(A)** Basal (non-postprandial) glycemia of 16-week-old mice fed on a chow diet (n = 17–24 per group) and on a HCD (n = 9–12 per group). **(B)** Basal (non-postprandial) serum insulin levels of 16-week-old mice fed on a chow diet (n = 9–15 per group) and on a HCD (n = 8–10 per group). **(C)** Intraperitoneal glucose (1.5 g/kg bodyweight) tolerance test and area under curve of mice at 11–13 weeks of age in the chow diet context (n = 6–8 per group). **(D)** Intraperitoneal glucose (1.5 g/kg bodyweight) tolerance test and area under curve of mice at 18–20 weeks of age in the HCD context (n = 5–10 per group). **(E)** Intraperitoneal pyruvate (2 g/kg bodyweight) tolerance test and area under curve of mice at 25–26 weeks of age in the chow diet context (n = 5–8 per group). **(F)** Intraperitoneal pyruvate (2 g/kg bodyweight) tolerance test and area under curve of mice at 26–28 weeks of age in the HCD context (n = 5–10 per group). Values are mean ± S.E.M. Panel A, B and C-F (area under curve): Statistics were analyzed using one-way ANOVA with Tukey correction for multiple comparisons (*$p < 0.05$). Panel C–F: Statistics were analyzed using repeated measures two-way ANOVA with Tukey correction for multiple comparisons (*$p < 0.05$, **$p < 0.01$, ****$p < 0.0001$ Wild-type *vs.* Sirt6BAC), (†$p < 0.05$, ††$p < 0.01$ Wild-type vs. Sirt6BAC; *Sirt6*$^{-/-}$), (‡$p < 0.05$, ‡‡‡$p < 0.001$ Sirt6BAC *vs.* Sirt6BAC; *Sirt6*$^{-/-}$).

expression and whole-blood polyamine content by qPCR and RP-HPLC, respectively. Our results indicate increased mRNA content of the glycolytic enzymes ATP-dependent 6-phosphofructokinase (PFKL) and liver-type pyruvate kinase (LPK) in liver of Sirt6BAC mice compared to wild-types (Figure S2). Furthermore, our data indicate increased mRNA content of Elovl6, Acetyl-CoA carboxylase-b (ACCb), and Fatty acid transport protein 5 (FATP5) in liver of Sirt6BAC mice compared to wild-types (Figure S2). However, we found no difference in serum triglyceride level between 16 and 20-week-old Sirt6BAC and wild-type mice fed on a standard diet (ng/dL; mean ± SEM: wild-types = 146 ± 12; Sirt6BAC mice = 139 ± 16; serum was collected from mice that were fasted over-night, n = 6 per group, $p > 0.05$).

Due to important role of polyamines on energy metabolism [30], we also assessed their level and found that total polyamines and spermidine contents are significantly higher in blood of Sirt6BAC mice compared to wild-types (Figure 7A,B). Collectively, these results suggest that SIRT6 overexpression improves glucose/insulin homeostasis in part by enhancing circulating spermidine contents and hepatic glucose and lipid metabolism.

4. DISCUSSION

Due to the staggering number of people suffering from defects in energy and glucose homeostasis and the shortcomings of current therapies, there is a pressing need for developing better approaches for the treatment of obesity and T2DM [1]. Several genetic studies have recently provided support for the idea that activation of SIRT1 (one of three mammalian nuclear sirtuin members) leads to improved metabolic homeostasis in the context of hyper-caloric feeding [8–11,31–34]. However, the role of another nuclear-localized sirtuin, namely SIRT6, in metabolism is controversial. Indeed, *Sirt6* loss- and gain-of-function studies have brought about counterintuitive and outwardly incongruent results, rendering it difficult to determine whether activation or inhibition of SIRT6 would result in beneficial metabolic outcomes [17–19,21–23,35]. These apparently paradoxical findings may be the result of the following non-mutually exclusive possibilities: i) reduced glycemia and body adiposity displayed by *Sirt6* null mice may not be direct consequence of SIRT6 deficiency, but secondary effects due to other serious abnormalities (e.g.: colitis, lymphopenia, etc.) caused by this mutation [17], ii) reduced glycemia and body

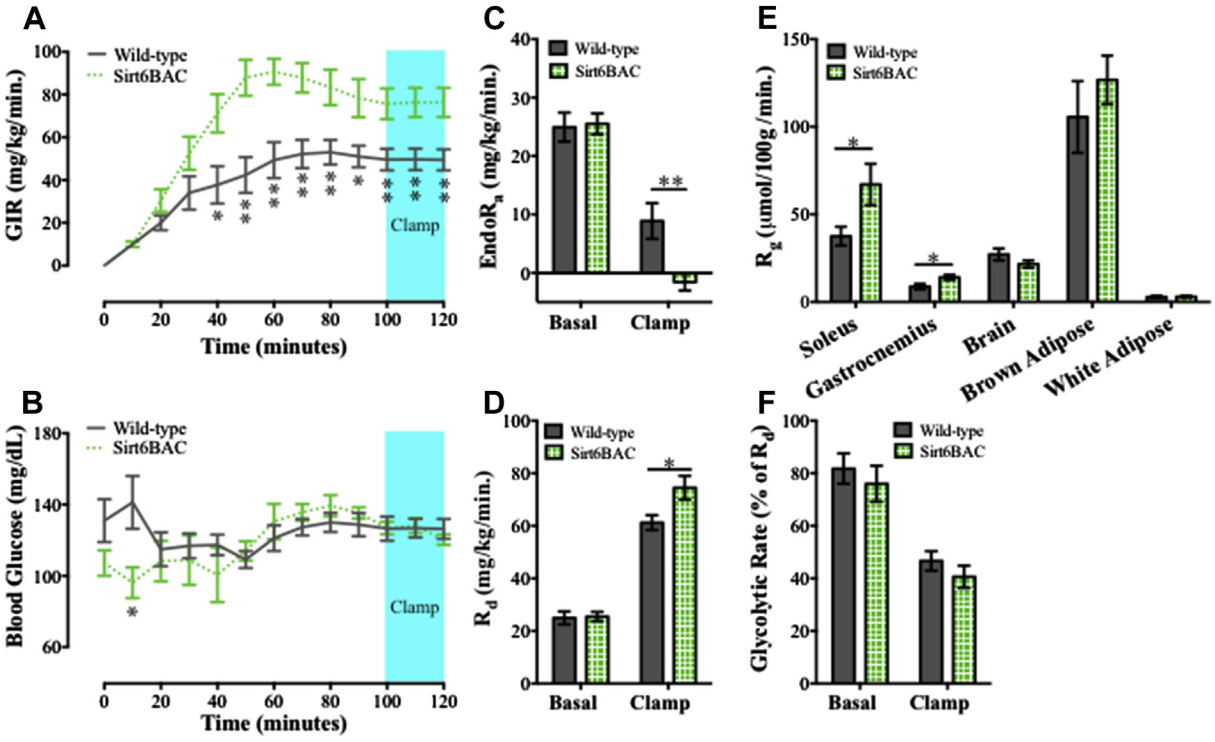

Figure 5: Sirt6BAC mice exhibit enhanced insulin sensitivity. **(A)** Glucose infusion rate (GIR) (mg glucose/kg bodyweight/minute) **(B)** Blood glucose (mg/dL) **(C)** Endogenous glucose appearance ($EndoR_a$) (mg/kg bodyweight/minute) **(D)** Glucose disposal (R_d) (mg/kg bodyweight/minute) **(E)** Tissue glucose uptake (R_g) (μmol/100 g tissue/minute) **(F)** Glycolytic rate (% of R_d). n = 6–8 per group. All mice were fed on a standard diet. Values are mean ± S.E.M. Panels A&B: Statistics were analyzed using repeated measures one-way ANOVA with Tukey correction for multiple comparisons (*p < 0.05, **p < 0.01). Panels C, D, E&F: Statistics were analyzed using unpaired two-tailed t-test (*p < 0.05, **p < 0.01).

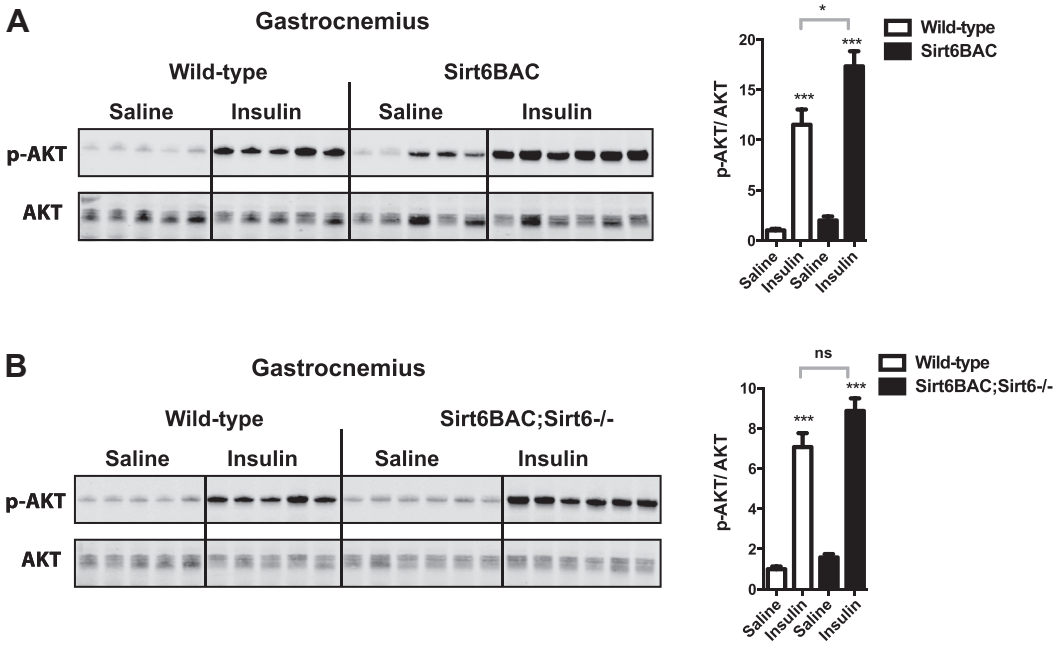

Figure 6: Sirt6BAC mice exhibit enhanced insulin-induced pAKT in gastrocnemius. Immunoblot and quantification of Akt (Thr^{308}) phosphorylation status relative to total AKT (AKT) in gastrocnemius muscle 10 min after an intraperitoneal bolus of insulin (5 U/kg) or saline in **(A)** wild-type *vs.* Sirt6BAC mice and **(B)** wild-type vs. Sirt6BAC; *Sirt6*$^{-/-}$ mice. All mice were fasted 5 h before insulin or saline injection. All mice were age-matched and fed on a standard diet. Error bars represent s.e.m. Statistical analyses were done using two-tailed unpaired Student's t test. *P < 0.05; ***P < 0.001.

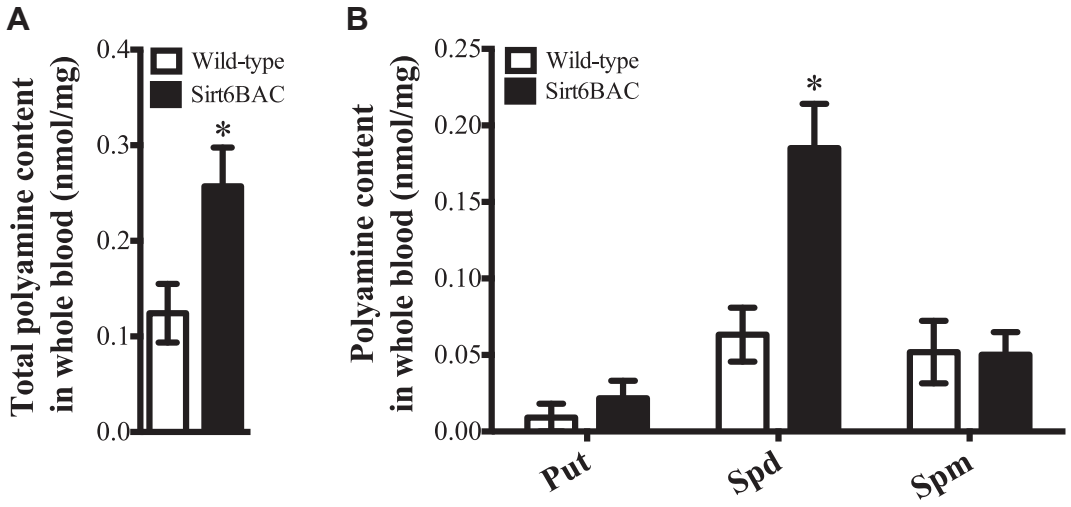

Figure 7: Sirt6BAC mice exhibit enhanced spermidine level in blood. (A) Total polyamine content and **(B)** polyamine profile of putrescine (Put), spermidine (Spd), and spermine (Spm) in whole blood of 2-month-old wild-type (n = 12) and Sirt6BAC (n = 7) mice fed on a standard diet. Error bars represent s.e.m. Statistical analyses were done using two-tailed unpaired Student's t test. *P < 0.05.

adiposity displayed by SIRT6-overexpressor mice may be due to inherent confounding effects of the unnatural chicken β*Actin* promoter/CMV enhancer-driven regulation of *Sirt6* expression in these mutants [22].

To gather insights about the effects of systemic and moderate activation of SIRT6, we genetically-engineered mice that eutopically and physiologically overexpress SIRT6. As the exogenously introduced *Sirt6* gene was under the control of its own natural promoter, SIRT6 overexpression in these Sirt6BAC mice mimicked SIRT6 expression in calorically restricted rodents (Figures 1 and S1) [29]. Importantly, the approach we used is strikingly different from the one Kanfi and colleagues employed. In fact, in the Kanfi and colleagues' model, the artificial chicken β*Actin* promoter/CMV enhancer drives *Sirt6* expression at non-physiological levels and probably in cell-types that would not normally express SIRT6 [22]. These shortcomings cast doubt on the interpretations of results gathered from this mutant. It is also important to note the limitations of our Sirt6BAC mouse model. The major caveat of this method is the presence of large genomic sequences flanking the mouse *Sirt6* gene (Figure 1A). While these large sequences are needed for *Sirt6* transcriptional fidelity, they also contain other known genes whose expression was also found to be increased in Sirt6BAC mice (Figure 1D). Hence, overexpression of these other genes could have contributed to the phenotypes displayed by Sirt6BAC mice. Also, BAC DNA construct insertion site(s) into the genome may have altered endogenous gene expression and hence caused phenotypes in Sirt6BAC mice. While the generation and study of another SIRT6 BAC line could be useful to address the latter this approach cannot address the former issue. In fact, the likelihood that two different BAC transgenic lines bear DNA construct cloned into the same genomic site(s) is virtually zero. Therefore, as expression of genes contained in the BAC likely depends on DNA construct insertion site(s) it is virtually impossible to assure equal expression of SIRT6 and also non-SIRT6 BAC-born products in different tissues of two different lines. Another approach would be to disrupt *Sirt6* sequences in BAC DNA construct and use this modified BAC DNA lacking the possibility to overexpress SIRT6 as a negative control line (hereafter referred to as Sirt6minusBAC mice). Again, while this approach is suitable to address potential insertion site effects, it cannot guarantee equal tissue-specific overexpression of BAC-born products between Sirt6minusBAC and Sirt6BAC mice. Hence, the Sirt6minusBAC mice cannot serve as controls to Sirt6BAC mice. On the other hand, BAC DNA insertion site is identical between Sirt6BAC; *Sirt6*$^{-/-}$ and Sirt6BAC mice. The only appreciable difference between these two lines is SIRT6 expression which in Sirt6BAC mice is enhanced while in Sirt6BAC; *Sirt6*$^{-/-}$ mice is almost normal (Figures 1B,C,D and S1). Hence, if a given phenotype were to be observed in Sirt6BAC mice and displayed at an intermediate degree or not displayed by Sirt6BAC; *Sirt6*$^{-/-}$ mice, then the given phenotype is very likely the consequence of *Sirt6* overexpression. Thus, to dissociate potential effects of BAC DNA insertion site and/or overexpression of non-SIRT6 BAC-born products to SIRT6 overexpression we used Sirt6BAC; *Sirt6*$^{-/-}$ mice as controls. Our study indicates that SIRT6 overexpression underlies the improved glucose/insulin profiles displayed by Sirt6BAC mice. This conclusion mainly rests on the following five observations: i) glycemia is significantly decreased in Sirt6BAC compared to wild-type HCD-fed mice; however, this phenotype is not displayed by Sirt6BAC; *Sirt6*$^{-/-}$ mice (Figure 4A), ii) following a bolus of glucose, the glycemic level over time is significantly decreased in Sirt6BAC compared to wild-type mice; however, this phenotype is not displayed by Sirt6BAC; *Sirt6*$^{-/-}$ mice (Figure 4C), iii) following a bolus of glucose, the glycemic level over time is significantly decreased in Sirt6BAC compared to wild-type HCD-fed mice; however, this phenotype is displayed at an intermediate degree by Sirt6BAC; *Sirt6*$^{-/-}$ mice (Figure 4D); iv) following a bolus of pyruvate, the glycemic level over time is significantly decreased in Sirt6BAC compared to wild-type HCD-fed mice; however, this phenotype is displayed at an intermediate degree by Sirt6BAC; *Sirt6*$^{-/-}$ mice (Figure 4F), v) the ability of insulin to induce phosphorylation of AKT is significantly increased in gastrocnemius of Sirt6BAC mice compared to wild-type controls; however, this phenotype is not displayed by Sirt6BAC; *Sirt6*$^{-/-}$ mice (Figure 6).

It is worth noting that some of our data are somewhat unexpected. For example, data shown in Figure 5D,E indicate that insulin-stimulated glucose disposal is enhanced in Sirt6BAC mice relative to wild-type controls. This is unexpected considering that loss of SIRT6 causes

enhanced glucose transporter-1 and -4 (GLUT1 and GLUT4) membrane localization and cell-autonomous glucose uptake [18,36]. The fact that our Sirt6BAC mice do not display changes in body adiposity (Figure 3) is not in keeping with Kanfi and colleagues' results as their *Sirt6* overexpressor model displays changes in this parameter [22]. While future studies may be needed to explain these differences, we suggest that these are the results of the different level and/or tissue distribution of *Sirt6* overexpression between our and Kanfi and colleagues' model [22].

In this study, we also attempted to shed light on potential mechanisms underlying the beneficial effect of SIRT6 on glucose homeostasis. Our results indicate that these pathways include increased circulating spermidine level and enhanced insulin sensitivity in liver and skeletal muscle (Figures 5–7). Of note, the improved hepatic insulin sensitivity of Sirt6BAC mice is in keeping with data indicating that SIRT6 inhibits the activity of the gluconeogenic co-transcription factor peroxisome proliferator-activated receptor-γ coactivator 1-α and with the fact that SIRT6 overexpression in liver improves hyperglycemia in diabetic mice [23]. SIRT6 has recently been shown to interact with proteins of the circadian core complex (e.g.: CLOCK and BMAL1) and to regulate expression of several clock-controlled genes [35]. Considering the important role of the circadian clock on metabolic homeostasis [37], it is formally possible that changes in circadian clock function in liver and skeletal muscle underlie the improved insulin sensitivity shown by Sirt6BAC mice. To fully determine the role of SIRT6 gain-of-function in specific tissues, future studies in tissue-restricted SIRT6 overexpressor mice are warranted.

5. CONCLUSIONS

In summary, our data indicate that moderate, physiological overexpression of SIRT6 enhances insulin sensitivity in skeletal muscle and liver, engendering protective actions against diet-induced T2DM. Hence, the present study provides support for the anti-T2DM effect of SIRT6 and may pave the way for the development of SIRT6 agonists aimed at treating T2DM.

DISCLOSURE SUMMARY

Authors have nothing to declare.

ACKNOWLEDGMENTS

We thank Carolyn Heckenmeyer, Ariane Widmer, and Anne Charollais in the Coppari laboratory for technical support, Dr. Raul Mostoslavsky at Harvard Medical School for providing the *Sirt6* null mice, the transgenic core facility at the University of Texas Southwestern Medical Center (USA), and Dr. Christelle Veyrat-Durebex at the glucose/insulin clamp platform at University of Geneva (Switzerland) (http://www.medecine.unige.ch/phenotypage/clampglucose.php). This work was supported by Coordenação de Aperfeiçoamento de Pessoal de Nível Superior (graduate student fellowship to R.M.I.), Juvenile Diabetes Research Foundation (Post-doctoral fellowship 3-2011-405 to T.F.), American Heart Association (Scientist Development Grant 14SDG17950008 to T.F.), European Commission (Marie Curie Career Integration Grant 320898 and ERC-Consolidator Grant 614847 to R.C.), and the Swiss National Science Foundation (310030_146533/1 to R.C.). This work has also received support from the Louis-Jeantet Foundation and the Fondation Pour Recherches Medicales of the University of Geneva (to R.C.).

CONFLICT OF INTEREST

None declared.

APPENDIX A. SUPPLEMENTARY DATA

Supplementary data related to this article can be found at http://dx.doi.org/10.1016/j.molmet.2015.09.003.

REFERENCES

[1] Vianna, C.R., Coppari, R., 2011. A treasure trove of hypothalamic neurocircuitries governing body weight homeostasis. Endocrinology 152(1):11–18.
[2] Coppari, R., Bjorbaek, C., 2012. Leptin revisited: its mechanism of action and potential for treating diabetes. Nature Reviews Drug Discovery 11(9):692–708.
[3] Maahs, D.M., Rewers, M., 2006. Editorial: Mortality and renal disease in type 1 diabetes mellitus–progress made, more to be done. The Journal of Clinical Endocrinology and Metabolism 91(10):3757–3759.
[4] Steffes, M.W., Sibley, S., Jackson, M., Thomas, W., 2003. Beta-cell function and the development of diabetes-related complications in the diabetes control and complications trial. Diabetes Care 26(3):832–836.
[5] Bluestone, J.A., Herold, K., Eisenbarth, G., 2010. Genetics, pathogenesis and clinical interventions in type 1 diabetes. Nature 464(7293):1293–1300.
[6] Ramadori, G., Lee, C.E., Bookout, A.L., Lee, S., Williams, K.W., Anderson, J., et al., 2008. Brain SIRT1: anatomical distribution and regulation by energy availability. The Journal of Neuroscience: The Official Journal of the Society for Neuroscience 28(40):9989–9996.
[7] Ramadori, G., Konstantinidou, G., Venkateswaran, N., Biscotti, T., Morlock, L., Galie, M., et al., 2015. Diet-induced unresolved ER stress hinders KRAS-driven lung tumorigenesis. Cell Metabolism 21(1):117–125.
[8] Ramadori, G., Gautron, L., Fujikawa, T., Vianna, C.R., Elmquist, J.K., Coppari, R., 2009. Central administration of resveratrol improves diet-induced diabetes. Endocrinology 150(12):5326–5333.
[9] Ramadori, G., Fujikawa, T., Fukuda, M., Anderson, J., Morgan, D.A., Mostoslavsky, R., et al., 2010. SIRT1 deacetylase in POMC neurons is required for homeostatic defenses against diet-induced obesity. Cell Metabolism 12(1):78–87.
[10] Ramadori, G., Fujikawa, T., Anderson, J., Berglund, E.D., Frazao, R., Michan, S., et al., 2011. SIRT1 deacetylase in SF1 neurons protects against metabolic imbalance. Cell Metabolism 14(3):301–312.
[11] Ramadori, G., Coppari, R., 2010. Pharmacological manipulations of CNS sirtuins: potential effects on metabolic homeostasis. Pharmacological Research 62(1):48–54.
[12] Coppari, R., Ramadori, G., Elmquist, J.K., 2009. The role of transcriptional regulators in central control of appetite and body weight. Nature Clinical Practice Endocrinology & Metabolism 5(3):160–166.
[13] Baur, J.A., Pearson, K.J., Price, N.L., Jamieson, H.A., Lerin, C., Kalra, A., et al., 2006. Resveratrol improves health and survival of mice on a high-calorie diet. Nature 444(7117):337–342.
[14] Lagouge, M., Argmann, C., Gerhart-Hines, Z., Meziane, H., Lerin, C., Daussin, F., et al., 2006. Resveratrol improves mitochondrial function and protects against metabolic disease by activating SIRT1 and PGC-1alpha. Cell 127(6):1109–1122.
[15] Ramadori, G., Coppari, R., 2011. Does hypothalamic SIRT1 regulate aging? Aging 3(3):325–328.
[16] Kugel, S., Mostoslavsky, R., 2014. Chromatin and beyond: the multitasking roles for SIRT6. Trends in Biochemical Sciences 39(2):72–81.
[17] Mostoslavsky, R., Chua, K.F., Lombard, D.B., Pang, W.W., Fischer, M.R., Gellon, L., et al., 2006. Genomic instability and aging-like phenotype in the absence of mammalian SIRT6. Cell 124(2):315–329.
[18] Zhong, L., D'Urso, A., Toiber, D., Sebastian, C., Henry, R.E., Vadysirisack, D.D., et al., 2010. The histone deacetylase Sirt6 regulates glucose homeostasis via Hif1alpha. Cell 140(2):280–293.

[19] Sundaresan, N.R., Vasudevan, P., Zhong, L., Kim, G., Samant, S., Parekh, V., et al., 2012. The sirtuin SIRT6 blocks IGF-Akt signaling and development of cardiac hypertrophy by targeting c-Jun. Nature Medicine 18(11):1643–1650.

[20] Hotamisligil, G.S., Shargill, N.S., Spiegelman, B.M., 1993. Adipose expression of tumor necrosis factor-alpha: direct role in obesity-linked insulin resistance. Science 259(5091):87–91.

[21] Jiang, H., Khan, S., Wang, Y., Charron, G., He, B., Sebastian, C., et al., 2013. SIRT6 regulates TNF-alpha secretion through hydrolysis of long-chain fatty acyl lysine. Nature 496(7443):110–113.

[22] Kanfi, Y., Peshti, V., Gil, R., Naiman, S., Nahum, L., Levin, E., et al., 2010. SIRT6 protects against pathological damage caused by diet-induced obesity. Aging Cell 9(2):162–173.

[23] Dominy Jr., J.E., Lee, Y., Jedrychowski, M.P., Chim, H., Jurczak, M.J., Camporez, J.P., et al., 2012. The deacetylase Sirt6 activates the acetyltransferase GCN5 and suppresses hepatic gluconeogenesis. Molecular Cell 48(6):900–913.

[24] Balthasar, N., Coppari, R., McMinn, J., Liu, S.M., Lee, C.E., Tang, V., et al., 2004. Leptin receptor signaling in POMC neurons is required for normal body weight homeostasis. Neuron 42(6):983–991.

[25] Lee, E.C., Yu, D., Martinez de Velasco, J., Tessarollo, L., Swing, D.A., Court, D.L., et al., 2001. A highly efficient Escherichia coli-based chromosome engineering system adapted for recombinogenic targeting and subcloning of BAC DNA. Genomics 73(1):56–65.

[26] Fujikawa, T., Berglund, E.D., Patel, V.R., Ramadori, G., Vianna, C.R., Vong, L., et al., 2013. Leptin engages a hypothalamic neurocircuitry to permit survival in the absence of insulin. Cell Metabolism 18(3):431–444.

[27] Berglund, E.D., Vianna, C.R., Donato Jr., J., Kim, M.H., Chuang, J.C., Lee, C.E., et al., 2012. Direct leptin action on POMC neurons regulates glucose homeostasis and hepatic insulin sensitivity in mice. The Journal of Clinical Investigation 122(3):1000–1009.

[28] Seiler, N., 1983. Liquid chromatographic methods for assaying polyamines using prechromatographic derivatization. Methods in Enzymology 94:10–25.

[29] Kanfi, Y., Shalman, R., Peshti, V., Pilosof, S.N., Gozlan, Y.M., Pearson, K.J., et al., 2008. Regulation of SIRT6 protein levels by nutrient availability. FEBS Letters 582(5):543–548.

[30] Kraus, D., Yang, Q., Kong, D., Banks, A.S., Zhang, L., Rodgers, J.T., et al., 2014. Nicotinamide N-methyltransferase knockdown protects against diet-induced obesity. Nature 508(7495):258–262.

[31] Price, N.L., Gomes, A.P., Ling, A.J., Duarte, F.V., Martin-Montalvo, A., North, B.J., et al., 2012. SIRT1 is required for AMPK activation and the beneficial effects of resveratrol on mitochondrial function. Cell Metabolism 15(5):675–690.

[32] Banks, A.S., Kon, N., Knight, C., Matsumoto, M., Gutierrez-Juarez, R., Rossetti, L., et al., 2008. SirT1 gain of function increases energy efficiency and prevents diabetes in mice. Cell Metabolism 8(4):333–341.

[33] Coppari, R., 2012. Metabolic actions of hypothalamic SIRT1. Trends in Endocrinology and Metabolism: TEM 23(4):179–185.

[34] Pfluger, P.T., Herranz, D., Velasco-Miguel, S., Serrano, M., Tschop, M.H., 2008. Sirt1 protects against high-fat diet-induced metabolic damage. Proceedings of the National Academy of Sciences of the United States of America 105(28):9793–9798.

[35] Masri, S., Rigor, P., Cervantes, M., Ceglia, N., Sebastian, C., Xiao, C., et al., 2014. Partitioning circadian transcription by SIRT6 leads to segregated control of cellular metabolism. Cell 158(3):659–672.

[36] Xiao, C., Kim, H.S., Lahusen, T., Wang, R.H., Xu, X., Gavrilova, O., et al., 2010. SIRT6 deficiency results in severe hypoglycemia by enhancing both basal and insulin-stimulated glucose uptake in mice. The Journal of Biological Chemistry 285(47):36776–36784.

[37] Sahar, S., Sassone-Corsi, P., 2012. Regulation of metabolism: the circadian clock dictates the time. Trends in Endocrinology and Metabolism: TEM 23(1):1–8.

